Biosensors and Bioelectronics 74 (2015) 214–221

Contents lists available at ScienceDirect

Biosensors and Bioelectronics

journal homepage: www.elsevier.com/locate/bios

Ultrasensitive strategy based on PtPd nanodendrite/nano-flower-like@GO signal amplification for the detection of long non-coding RNA

Fei Liu [a], Guiming Xiang [a], Dongneng Jiang [a], Liqun Zhang [a], Xuemei Chen [b], Linlin Liu [a], Fukang Luo [a], Yi Li [a], Chang Liu [a], Xiaoyun Pu [a,*]

[a] Department of Clinical Laboratory, Xinqiao Hospital, Third Military Medical University, Chongqing 400037, China
[b] Shima River Community Health Center, Jiangbei District, Chongqing 400021, China

ARTICLE INFO

Article history:
Received 24 March 2015
Received in revised form
19 May 2015
Accepted 7 June 2015
Available online 23 June 2015

Keywords:
Long non-coding RNA (lncRNA)
Highly up-regulated in liver cancer (HULC)
PtPd bimetallic nanodendrites/nanoflower-like clusters on graphene oxide (PtPd BND/BNF@GO)
Biosensor

ABSTRACT

Highly up-regulated in liver cancer (HULC) is a novel promising noninvasive biomarker for hepatocellular carcinoma (HCC), which is a kind of long non-coding RNAs (lncRNAs). But traditional methods limited HULC clinical detection for ownself drawbacks. Development a new HULC detection approach is urgent and necessary. Electrochemical nucleic acid sensor based on different signal amplification strategies with high sensitivity, fast, simple, and convenient, may solve this problem. Herein, we propose a novel strategy based on Pt–Pd bimetallic nanodendrites/nanoflower-like clusters on graphene oxide/Au/horseradish peroxidase (PtPd BND/BNF@GO/Au/HRP) to enhance the catalytic efficiency and sensitivity. And Au particles were simultaneously and separately capped with thionine or detection probe, which increase the binding amount of detection probe and decrease the electronic background. The results indicated that the catalytic effect was noticeably elevated and that the biosensor provides ultrasensitive detection for the lncRNA HULC. The linear calibration of the biosensor ranged from 1.00×10^{-3} to 1.00×10^{3} pM/mL, and the limit of detection was 0.247 fM/mL. The lncRNA biosensor based on the PtPd BND/BNF@GO/Au/HRP/Au/thionine exhibited acceptable reproducibility and clear selectivity. This strategy may provide a new alternative for clinical HCC diagnosis through the detection of HULC.

1. Introduction

Hepatocellular carcinoma (HCC) is the fifth most common cancer in men and the seventh in women worldwide, which causes more than 662,000 deaths worldwide each year (Ferlay et al., 2010; Siegel et al., 2014). Highly up-regulated in liver cancer (HULC) dramatically up-regulated in HCC (Panzitt et al., 2007) is a long non-coding RNA (lncRNA), which represent a subgroup of longer than 200 nucleotides non-coding RNAs (Yuan et al., 2012). It can be used as a noninvasive promising novel biomarker for the diagnosis of HCC (Xie et al., 2013). Although there are several traditional methods, inherent drawbacks of those methods limited the clinical application of HULC. For instance, *rt*-PCR limits a certain optimal linear range and requires specialized personnel and equipment. Northern blot is harmful to the body and environment for radioactive probe. Co-IP can only detect protein binding lncRNA, not including HULC. Electrochemical biosensor which is high sensitivity, fast, simple, and convenient based on various types of nanomaterials may provide an alternative way for HULC detection (Centi et al., 2009; Holford et al., 2012). Meanwhile, there are no reports about HULC detection with biosensors. So development electrochemical biosensor for HULC detection is important and necessary.

To improve the sensitivity of electrochemical DNA biosensors, signal amplification strategies based on various bio-nanocomposite probes have been proposed that involve loading a large amount of electrochemical mediators and natural enzymes onto nanomaterials.

Single-wall carbon nanotubes (SWCNTs) have been incorporated into electrochemical sensors because of their remarkable tensile strength, high resilience, large surface area, flexibility and other unique structural, mechanical, electrical and physicochemical properties (Daniel et al., 2007). SWCNT-based sensors generally exhibit higher sensitivities, lower limits of detection, and faster electron-transfer kinetics than traditional electrodes (Jacobs et al., 2010). Graphene oxide (GO) as a 2-dimensional material has received increasing attention because of its unique physicochemical properties (e.g., high surface area, excellent conductivity, high mechanical strength, and ease of functionalization and mass production) (Shao et al., 2010), being an excellent material for electro analysis and catalysis.

* Corresponding author.
E-mail address: puxiaoyong63@sina.com (X. Pu).

http://dx.doi.org/10.1016/j.bios.2015.06.021
0956-5663/

In additional, noble metal nanoparticles are known to increase sensitivity and selectivity of biosensor and yield fast response times toward H_2O_2 (Doria et al., 2012; Wang, 2012). For instance, platinum (Pt) and palladium (Pd) possess advantages including higher specific surfaces, better catalytic properties, stability, biocompatibility and size-related electronic properties (Liang et al., 2004; Vasquez et al., 2005). So both have been widely used in biosensor (Liu et al., 2015; Zhu et al., 2015). But besides the composition, the surface structure which is determined by their shape, to a large extent is also important (Zhang et al., 2011; Zhou and Li, 2012). Tremendous efforts have been made to synthesize bimetallic nanocomposites with different morphologies, such as cubes, octahedra, and tetrahedra, to regulate their surface structure.

To achieve better detection, most electrochemical biosensors require label electroactive indicators, for instance, thionine (Li et al., 2015), which is a small electroactive molecule that contains two amine groups (Zhu et al., 2012). However, thionine is difficult to directly bind to HULC for no related residues in nucleic acids. Therefore, a series of labeling methods that indirectly absorb other materials, such as graphene (Lai et al., 2014; Li et al., 2015), electrode coatings (Wu et al., 2013) and SWCNT (Gong et al., 2008; He et al., 2006), have been developed. But the high signal background is a notable drawback and may hinder the specificity of detection. Recently, another labeling method was developed that employed thionine-capped Au particles because the nitrogen atoms of the $-NH_2$ moieties of thionine strongly bind to AuNP surfaces (Liu et al., 2011; Yang et al., 2014; Yuan et al., 2010).

Herein, we proposed a novel strategy based on Pt–Pd bimetallic nanodendrites/nanoflower-like clusters on GO (PtPd BND/BNF @GO) stereochemical structure to enhance the catalytic efficiency toward H_2O_2 in cooperation with horseradish peroxidase (HRP) to form a triple catalysis strategy (Pt, Pd and HRP). The application of GO may prompt the amount of loading of the PtPd BND/BNF. The strategy of thionine and detection probes synchronously and separately capping Au particles was employed, which notably accelerated the modification time of the detection probe and decreased the electronic background. Compared with traditional *rt*-PCR, the proposed biosensor exhibited high sensitivity, good reproducibility, acceptable stability and ideal selectivity and is an economical and rapid quantitative alternative for lncRNA HULC detection. Therefore, the strategy shows potential application of the clinical early diagnosis for HCC.

2. Experiment

2.1. Reagents

Pt chloride (H_2PtCl_6), gold chloride tetrahydrate ($HAuCl_4$), potassium palladium (II) chloride (K_2PdCl_4), poly-(vinylpyrrolidone) (PVP), poly(diallyldimethylammonium chloride) (PDDA), NaOH, and cyclohexanethiol (HT) were purchased from Sigma Chemical Co. (St. Louis, MO, USA). Phosphate buffered solution (PBS) (pH 7.4) was prepared using 0.1 M Na_2HPO_4 and 0.1 M KH_2PO_4. The prepared solutions were maintained at 4 °C before use. Seven cases of human blood serum samples were collected from the Department of Clinical Laboratory of Xinqiao Hospital with the informed consent of the patients. GO was purchased from Nanjing Xianfeng Nano Co. (Nanjing, China). The buffer for the preparation of the lncRNA probe solutions was tris–EDTA buffered solution (TE buffer) (10 mM Tris–Cl, pH 7.4, containing 1 mM EDTA).

HULC was adopted in this research as a representative lncRNA molecule because of its important role in liver cancer. Sulfhydryl-modified capture probe (CP) (5′-GTTCGGTCCTTCTCA-(CH_2)6-SH-3′) was designed to hybridize the target RNA near the 5′ end of the sequence. The target RNA (5′-TGAGAAGGACCGAACGTCTAACCC CGGAACGAC GACAT-3′) and sulfhydryl-modified detection probe (DP) (5′-SH-(CH_2)3-GTTCGGTCCTTCTCA-3′) were synthesized by Shanghai Sangon Biotechnology Co. (China).

miRNA-16 (5′-CTCAACTGGTGTCGTGGAGTCGGCAATTCAGTT-GAGCGCCAATA-3′), *β-actin* (5′-TGACGTGGACATCCGCAAAG-3′) and *gapdh* (5′-GATGGGATTTCCATTGATGACA-3′) were used as interfering substances.

2.2. Apparatus

Cyclic voltammetric (CV), electrochemical impedance spectroscopy (EIS) and differential pulse stripping voltammetry (DPV) measurements were performed using a CHI 660d electrochemistry workstation (Shanghai CH Instruments, Shanghai, China). The three-compartment electrochemical cell contained a platinum wire auxiliary electrode and a saturated calomel reference electrode (SCE). The working electrode was a glassy carbon electrode (GCE, diameter 4 mm) electrode. Transmission electron microscopy (TEM) measurements were performed on a JEM-1400 (JEOL, Tokyo, Japan) and TECNAI 10 (Philips Fei Co., Hillsboro, OR). pH measurements were performed with a pH meter (MP 230, Mettler-Toledo, Switzerland) and a digital ion analyzer (Model PHS-3C, Dazhong Instruments, Shanghai, China). Atomic Force Microscope (AFM) measurements were performed on Bruker Multimode 8 (Karlsruhe, German).

2.3. Synthesis of Au particles

The Au particles were synthesized according to the classic Frens method (Frens, 1973). First, 1% of $HAuCl_4$ and 1% of sodium citrate ($Na_3C_6H_5O_7$) solution were prepared separately. Then, 25 mL of $HAuCl_4$ was heated to boiling under vigorous stirring, and 1.5 mL of $Na_3C_6H_5O_7$ solution was added; boiling was continued for 30 min, and the solution was allowed to naturally cool to room temperature. The color of solution became red, yielding Au nanoparticles.

2.4. Preparation of GO and SWCNT

First, 7 mg of GO was dispersed in 14 mL of distilled H_2O. Then, ultrasonic stirring was performed for 2 h to obtain a 0.5 mg/mL GO solution. Next, 8 mg of SWCNTs was added to 16 mL of H_2O followed by the addition of 267 μL of 30% PDDA ($Mw < 10{,}000$) to obtain a 0.5 wt% PDDA solution. The solution was ultrasonically stirred to obtain a stable PDDA–SWCNTs suspension (0.5 mg/mL).

2.5. Synthesis of PtPd BND/BNF@GO

The procedure was modified based on a previously reported synthetic method (Bin et al., 2014; Guo et al., 2010; Lv et al., 2014). The PVP-stabilized PtPd BND/BNF@GO was synthesized using a one-pot method, with $NaBH_4$ as the reducing agent. The preparation process was as follows: 20 mg of PVP was dissolved in 2.0 mL of water accompanied by vigorous stirring for 10 min. Then, 3 mL of 0.5 mg/mL GO solution was added, and stirring was continued for 30 min. Then, 150 μL of 2 M NaOH was added to adjust the pH to achieve alkalinity. Next, 800 μL of H_2PtCl_6 (1%) and 600 μL of K_2PdCl_4 (1%) were added under stirring for 0.5 h. Subsequently, 10 mL of freshly prepared $NaBH_4$ (2 mg/mL) aqueous solution was added dropwise under vigorous stirring for 1 h at ambient temperature. The resulting blackturbid liquid was centrifuged and repeatedly washed with deionized water and ethanol to remove excess $NaBH_4$, which was dispersed in the 3 mL of deionized water.

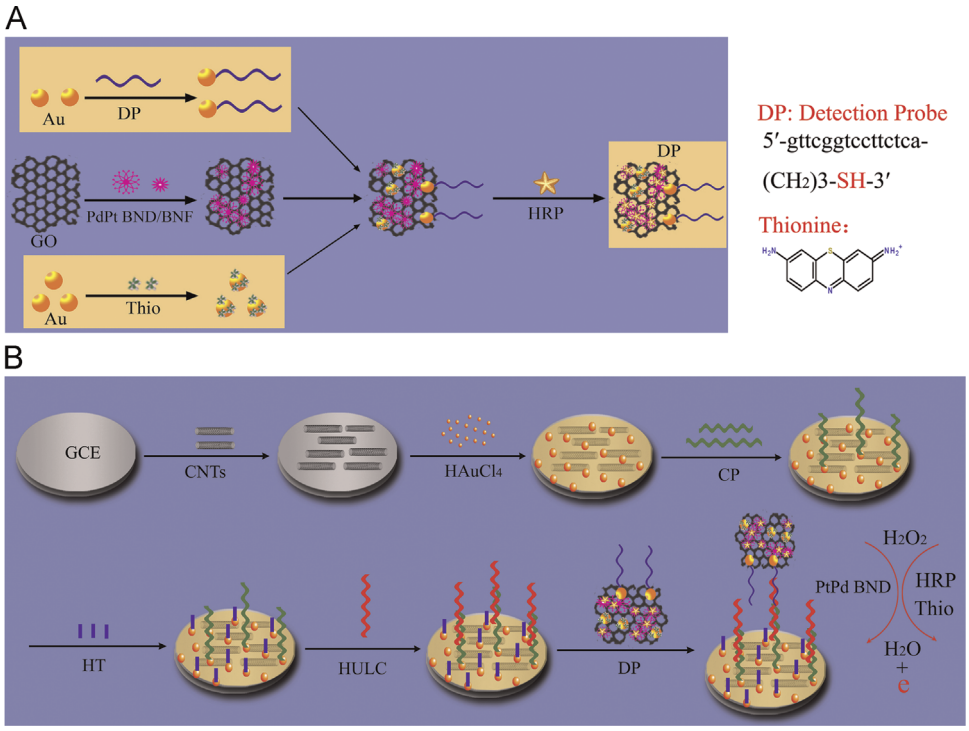

Scheme1. Schematic diagram of sandwich fabrication and detection of the lncRNA HULC biosensor.

2.6. Preparation of DP adsorbed nanomaterial

Thionine-capped AuNP was prepared according to references (Liu et al., 2014; Tang et al., 2008). The AuNP particle solution (1.0 mL) (seen in Fig. S1) was mixed with 0.025 mL of thionine aqueous solution (40 mM) and stirred effectively for 12 h. The solution was then centrifuged at 12,000 rpm for 10 min to obtain the precipitate of thionine-capped AuNP conjugates. Then, the precipitate was washed several times with double distilled water. The precipitate was re-dispersed easily in water via sonication. Unbound thionine was removed from the thionine-capped AuNP conjugate solutions by repeated washing and centrifugation (Scheme 1A).

The proposed DP bioconjugate was prepared as follows (Scheme 1A): the AuNP particle solution (0.5 mL) was mixed with 20 μL of HULC DP(100 μM) and stirred overnight. Then, the excess DP was removed by repeated centrifugation with distilled water washing. The precipitate was resuspended in 0.5 mL of distilled water. Finally, 0.5 mL of thionine-capped AuNP conjugates and 2 mL of PtPd BND/BNF@GO were added, and stirring was continued for 10 h. Subsequently, HRP was added into the solutions to reduce the nonspecific adsorption through blocking excess binding sites. After being centrifuged at 5000 rpm for 10 min, the supernatant was discarded, and the precipitate was resuspended. This step was repeated three times. Finally, the precipitate was resuspended in 1.2 mL of distilled water.

2.7. Fabrication of the biosensors

Before electrodes modification, each bare glassy carbon electrodes (GCE) was firstly polished with 0.3 μm alumina slurry for 5–10 min, then rinsed with deionized water. After that, GCE was subsequently polished by 0.05 μm alumina slurry for the similar time and rinsed with deionized water. Then sonicated in deionized water for 1–2 min, and dried with a high-purity nitrogen stream to obtain a clear electrode surface. The fabrication process of the biosensor is illustrated in Scheme 1B. The best effect of SWCNT modification is just to be formed a film on a glassy carbon electrode. So firstly, 8 μL of SWCNT solution (1 mg/mL, seen in Fig. S1) was dropped on the GCE for 8 h at room temperature to form a film. After the electrode dried, Au particles were directly deposited on the electrode, and CVs were obtained in 100 μM/L $HAuCl_4$ by stripping analysis for 30 s. The SWCNT/Au composite was used as an operational matrix to immobilize the HULC CP via gold–sulfur bonds. Next, the proposed electrode was incubated in 15 μL of HT solution (2 mM) for approximately 50 min to block the possible non-modified Au surface and eliminate any non-specific absorption. After washing the modified electrode surface, 15 μL of different concentrations of lncRNA HULC solution was added, and the solution was incubated at 25 °C for 3 h. Then, 20 μL of the HULC DP solution was added to the electrode surface and incubated for 3 h.

2.8. Experimental measurements

Electrochemical experiments were performed in a conventional electrochemical cell containing a three-electrode arrangement. CV and EIS measurements of the electrode fabrication were performed in 5 mM $[Fe(CN)_6]^{3-/4-}$ solution containing 0.1 M KCl. DPV was performed in 2 mL of 0.1 MPBS (pH 7.4) with the participation of an appropriate amount of H_2O_2 as the substrate from −0.6 to 0 V with a sweeping rate of 50 mV/s.

3. Results and discussion

3.1. TEM and XPS analysis of the PtPd BND/BNF@GO

Fig. S1A and B show the morphology of GO at low and high magnification, respectively. The TEM results indicated that hydrated GO exhibits the typical wrinkle morphology.

The TEM images (Fig.1) reveal the typical morphology of the synthesized PtPd nanomaterial. The PtPd BND/BNF@GO with controllable size or different numbers of dendrites or branches

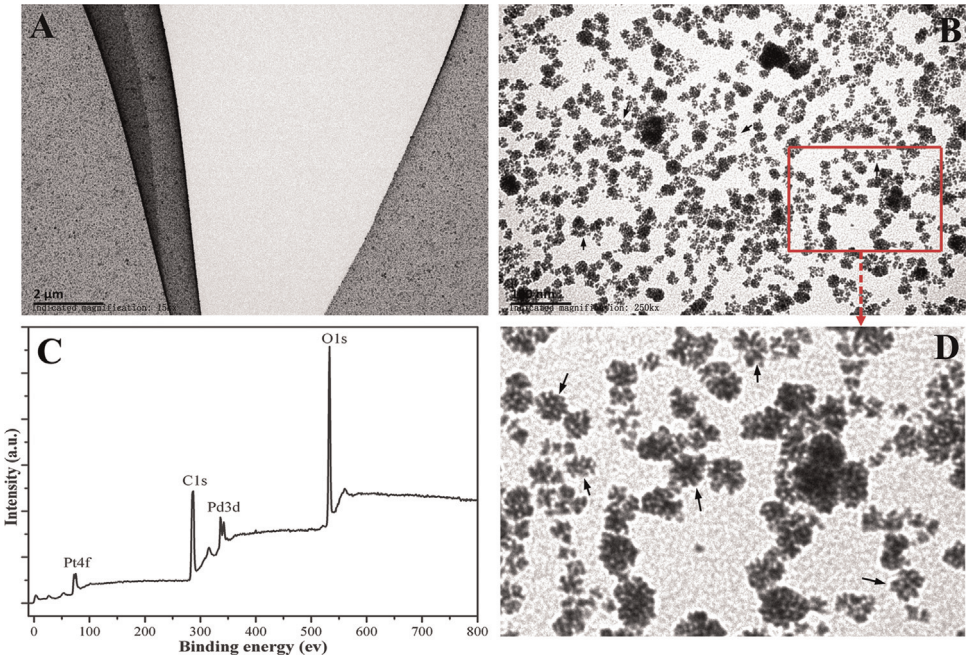

Fig. 1. (A–B) TEM images of PtPd BND/BNF@GO at various magnifications: A: 1500 ×, B:250,000 ×, C: XPS pattern of PtPd BND/BNF@GO , and D: magnified view of the rectangle pane in B.

adheres to the GO nanosheets (Fig. 1A). As indicated by the arrows in Fig. 1B and D, the typical shape of the nanomaterial mainly consisted of a dendritic structure, mixed with a small part of a cluster or snow-flower like. The nanodendritic structures are composed of many small branches and exhibit bifurcation architecture, with a length ranging from 10 to 40 nm and a width ranging from 5 to 20 nm, which is in agreement with previously reported results (Guo et al., 2010; Lim et al., 2009; Wang et al., 2011). The PtPd nanocluster shapes are snowflake-like or catkin-like, with nanobranches diverging from the center, which is similar to the results reported by Lv et al., (2014). The sizes of the snowflake-like nanoclusters are approximately 20 nm, and their branches are approximately 10–30 nm in length and 3–6 nm in width in various directions. As observed from the large-field angle, the nanodendrites and nanoclusters are not evenly distributed and tend to form a broken line or segment line. Therefore, a mesh and blank with different sizes would form, which may be correlated with PVP, which exhibit a long polymeric chain structure as the surface stabilizer (Shin et al., 2004; Vasquez et al., 2005).

XPS analysis provided information about the chemical composition of PtPd BND/BNF@GO. As depicted in Fig. 1C, the peaks located at 72.08, 287.08, 336.08 and 553.08 eV are assigned to the binding energies of Pt_{4f}, C_{1s}, Pd_{3d} and O_{1s}, respectively, demonstrating the coexistence of Pt, Pd and GO.

In the real fabrication of biosensor, the PtPd BND/BNF@GO is seven to eight times to AuNP nanoparticle that used to label thionine and CP. In additional, the biosensor after modified PtPd BND/BNF@GO-DP, the biosensor was swept 10 laps in 5 mM of $[Fe(CN)_6]^{3-/4-}$ solution, the signal is still very stable. Moreover, the biosensor sweep in 5 min, 10 min and 15 min after modification with CV methods, the current changed little.

3.2. *Electrochemical characteristics of the stepwise modified electrodes*

The CVs were analyzed in 0.10 M PBS containing 5 mM $K_3Fe(CN)_6$ and $K_4Fe(CN)_6$ (pH 7.4) in the potential range from −0.2 to 0.6 V at a scan rate of 50 mV/s (Fig. 2A). Curve a represents the bare GCE, which contains a typical pair of reversible redox peaks that correspond to the reversible redox reaction of the bare GCE, and curve b represents the SWCNT nanofilms; the redox peak currents of curve b increased 19.93% ($\Delta I = 27.41$ μA) compared with those of curve a, which implies that the SWCNTs exhibited good conductivity. The peak current increased 4.3% ($\Delta I = 7.10$ μA,

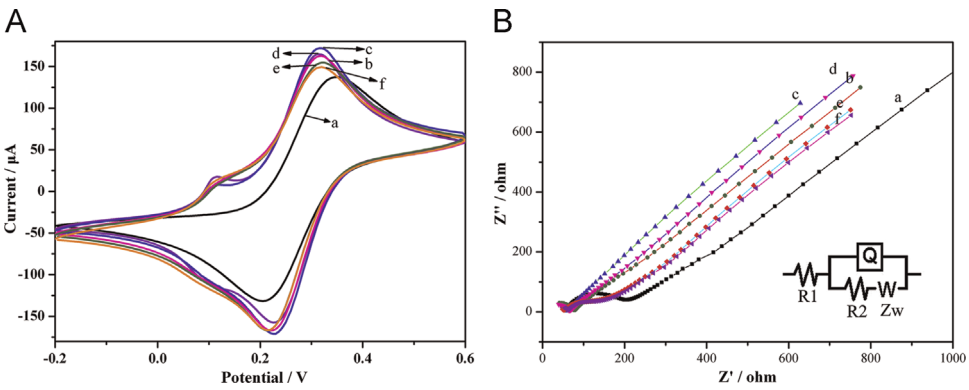

Fig. 2. CVs (A) and Nyquist diagrams (B) for the modified electrodes step by step; the CVs were obtained in $[Fe(CN)_6]^{3-/4-}$. Curve a, bare GCE; curve b, drop SWCNTs; curve c, electrodeposition Au; curve d, SWCNTs/Au/CP; curve e, SWCNTs/Au/CP/HT; curve f, SWCNTs/Au/CP/HT/HULC.

curve c) after Au was electrodeposited, indicating that Au was successfully deposited on the electrode. The electrode was subsequently incubated with the HULC CP, and the redox peak current decreased by 9.47 μA (a decrease of 5.47%, curve d), which implies that a considerable amount of CP was immobilized on the Au surface through Au–S bonding. After the electrode was blocked with HT (curve e), the peak currents were decreased due to HT electron hindrance (4.92%, $\Delta I = -8.05$ μA). Curve f represents the SWCNTs/Au/CP/HT/HULC; the peak currents associated with curve e decreased compared with those associated with curve d (3.43%, $\Delta I = -5.31$ μA). The CV results indicated that the series of nucleotide sequences or impacting medium (i.e., CP, HULC, and HT) readily bound to the electrode.

The CV results were further confirmed by EIS characterization, which is an effective method for studying the interface properties of surface-modified electrodes and the electron-transfer resistance at an electrode surface. As depicted in Fig. 2B, curve a represents bare GCE; the resistance decreased considerably after the electrode was modified with SWCNTs and Au (curves b and c, respectively). In contrast, after the electrode was incubated with HULC CP, the resistance notably increased because of the poor conductivity of CP (curve d); this result was supported by the aforementioned CV characterization. Curve e represents HT, and curve f represents the target HULC. As expected, both resistances continued to increase. The equivalent circuit model was fitted by Simpwin, as shown in the inset of Fig. 2B. The equivalent circuit model contains R_1, R_2, Zw and Q. R_2 and Zw are connected in series and both are parallel with Q ($Chisq = 1.96 \times 10^{-3}$, $P < 0.01$). The first resistance is related to the electrical behavior of the solution (R_1). The resistance R_2 is related to charge transfer of the electrode membrane, and Zw is the Warburg impedance, which is related to the mass transfer.

The CV and EIS characterization both revealed that these proteins were successfully modified on the electrode, implying that the proposed nucleic acid biosensor exhibited excellent loading capacity.

Moreover, the fabrication process was investigated by AFM. As showed in Fig. 3A with the AFM 3D image, the surface of the

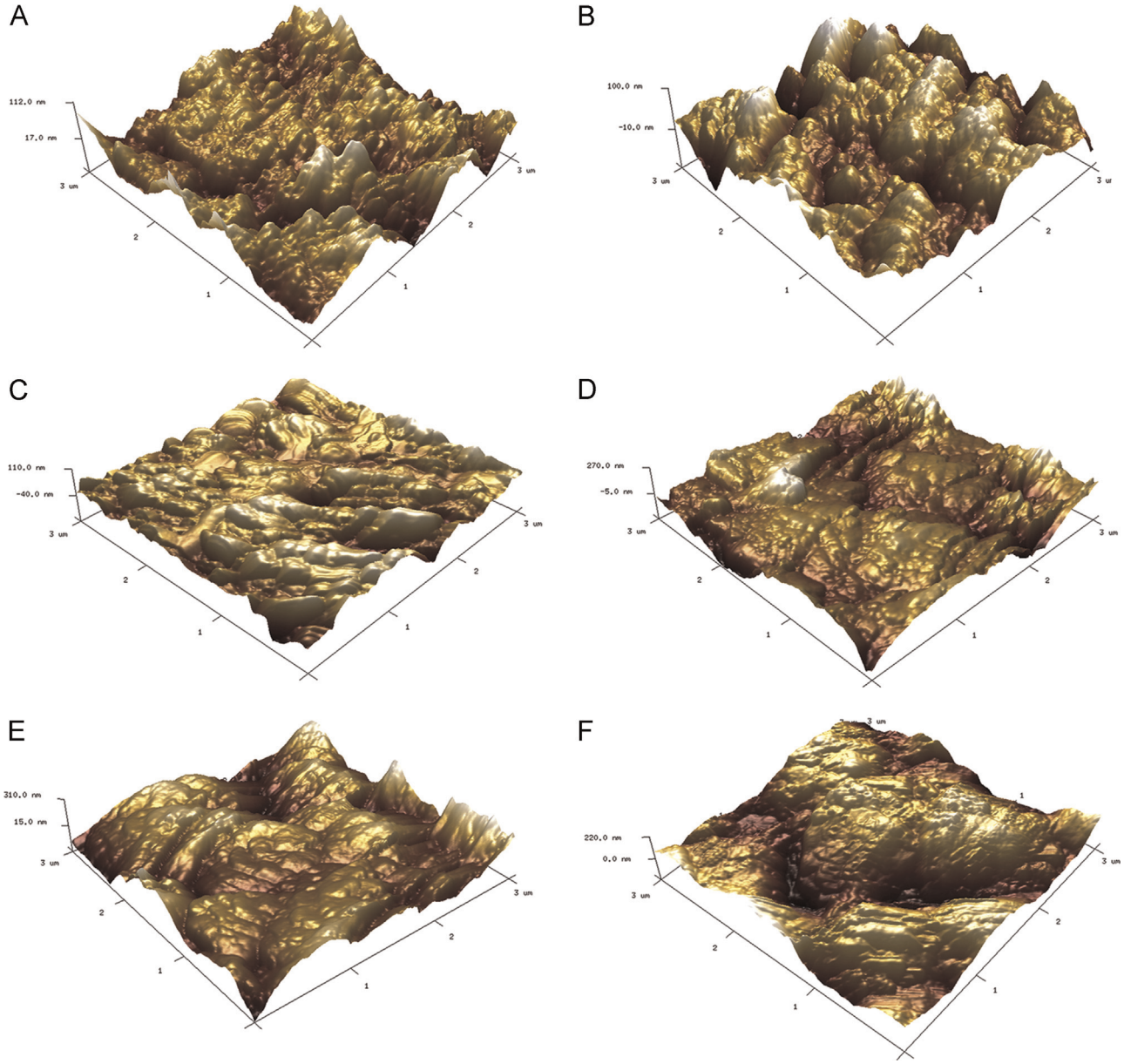

Fig. 3. AFM 3D images of SWCNTs (A), electrodeposition Au (B), SWCNTs/Au/CP (C), SWCNTs/Au/CP/HT (D); SWCNTs/Au/CP/HT/HULC (E), modified electrode biosensor reacted with DP linked Thi-Au/PtPd BND/BNF@GO/HRP (F).

SWCNT was undulating mountains irregularly with root mean square (RMS) roughness of 22.9 nm. After electrodeposition with a nano-Au layer (Fig. 3B), there were some small particle-like morphology on the surface with an increased RMS roughness of 136.5 nm as the modification of nano-Au onto the SWCNT modified electrode. The RMS roughness decreased to 27.1 nm indicating the surface became relatively smooth due to the adsorption of DNA onto the nano-Au modified surface (Fig. 3C). Furthermore, the RMS roughness obviously increased to 69.4 nm in the image of proposed biosensor as blocked with HT (Fig. 3D). When binding to target HULC, the RMS increases a little (72.4 nm, Fig. 3E). After biosensor reacted with signal probe linked Thi-Au/PtPd BND/BNF@GO/HRP nanocomposites, the RMS increased to 95.7 nm (Fig. 3F), indicating the presence of PtPd BND/BNF@GO related nanocomposite successfully reacted onto the surface of the proposed biosensor. All of these results obtained seem to further supported the successful fabrication and potential application for the proposed biosensor.

3.3. Comparison of the effect of Au particles with and without the thionine-cap on the electrochemical characteristics

To investigate the origin of the final signal, we compared different labeled probes and the amplification performance of the thi-Au/PtPd BND/BNF@GO/Au/DP/SWCNT/Au and PtPd BND/BNF@GO/Au/DP/SWCNT/Au. As observed in Fig. S3, changes in the current using the simple thionine-capped Au particle approach are apparent. Curve a represents the DP without thionine-capped Au particles, and curve b represents the DP with thionine-capped Au particles. The current response was detected in 0.1 M PBS (pH 7.4) because of the thionine electroactive indicator, indicating that the indirect labeled approach is feasible.

3.4. Optimization of analytical conditions

Based on the CV measurements and multiple optimizations, 2 μM concentration of CP and 8 h of incubation time were applied in this experiment for the probe immobilization (Fig. S4).

Subsequently, the effect of reaction solution pH for the sensor response was examined. Fig. S5 presents the CV plot of the fully assembled biosensor under exposure to 10 fM/mL HULC in 2 mL of 0.1 M PBS buffer solution with different pH containing H_2O_2. The pH of the working buffer was evaluated by adding the proposed biosensor to working buffer solutions with pH varying from 5.0 to 8.0 (Fig. S5A). The results indicate that the maximum peak current response was obtained at pH 7.0. Thus, PBS with pH 7.0 was employed as the optimum condition and was used as the working buffer for further studies.

In addition, the concentration of H_2O_2 in the detection solution was tested by CV for various concentrations of H_2O_2 based on the biosensor reacted with 10 fM HULC (Fig. S5B). The results indicated that the current responses increased with an increasing concentration of H_2O_2 up to 0.8 mM and then tended to plateau. Therefore, 0.8 mM H_2O_2 was adopted as the optimum concentration for further studies.

3.5. The signal amplification strategies of different conjugates

The signal amplification was derived from the Pt–Pd BND/BNF@GO nanocomposites and the HRP simultaneously acting as catalytic catalase. To evaluate the effect of the final signal, we compared different labeled probes and the amplification performance of the SWCNTs/Au/CP/HT/HULC/GO/Thio/Au/DP/HRP and SWCNTs/Au/CP/HT/HULC/PtPd BND/BNF @GO/Thio/Au/DP/HRP electrodes. As a result, the DNA biosensor with PtPd BND/BNF@GO/Thio/Au/DP/HRP probes exhibited the maximum response current indicating the PtPd BND/BNF could effectively improve the supporting amount of electron mediator electro catalytic complex (Fig. S6). On the basis of these results, we might make the conclusion that the the Pt–Pd BND/BNF@GO nanocomposites and the HRP system could be utilized for amplifying the electro-chemical signal.

3.6. Calibration line for HULC with the RNA biosensor

The as-prepared electrochemical RNA biosensor was incubated with various HULC concentrations. The top curve in Fig. 4 represents the baseline; the other curves from top to bottom represent different concentrations ranging from 1.00×10^{-3} pM/mL to 1.00×10^{3} pM/mL. We selected eight concentrations: 1.00×10^{-3}, 5.00×10^{-3}, 1.00×10^{-2}, 1.00×10^{-1}, 1.00, 1.00×10^{1}, 1.00×10^{2} and 1.00×10^{3} pM/mL. As the HULC concentration increased, the cathodic peak current clearly increased because the signal was notably amplified by the PtPd BND/BNF and HRP in the presence of H_2O_2. Furthermore, the data were analyzed using statistical correlation calculations, and a linear relationship was observed between the cathode peak current and HULC concentrations in the range of 1.00×10^{-3} to 1.00×10^{3} pM/mL. The linear equation was $I = -3.89 \log C_{HULC} - 17.04$, with a correlation coefficient of 0.9979. The detection limit was determined to be 0.247 fM/mL based on the $3\,s/\kappa$ rule (where s is the relative standard deviation of a blank solution and κ is the slope of the corresponding calibration curve).

Furthermore, a comparison of the performances of several types of biosensors used for the detection of non-coding RNA is presented in Table S1. The proposed biosensor exhibits a

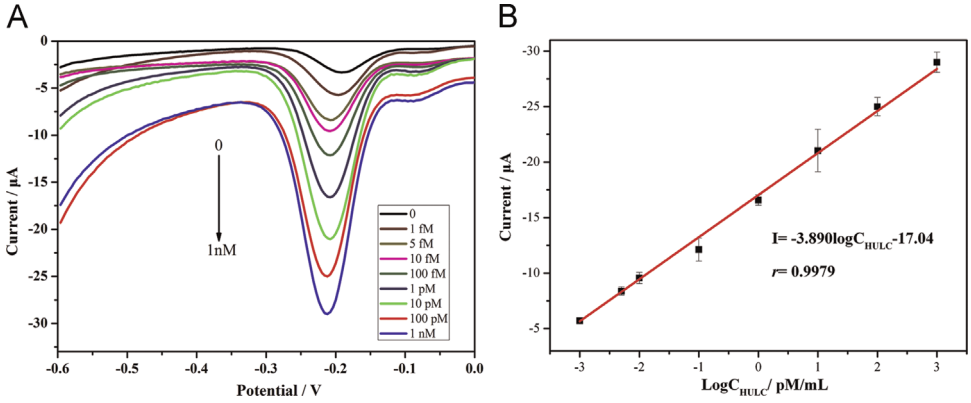

Fig. 4. Calibration plots of the cathodic peak current response vs. the HULC concentration. The inset shows the CVs of the cathodic peak at various concentrations (from top to bottom: 0, 1.00×10^{-3}, 5.00×10^{-3}, 1.00×10^{-2}, 1.00×10^{-1}, 1.00, 1.00×10^{1}, 1.00×10^{2}, and 1.00×10^{3} pM/mL).

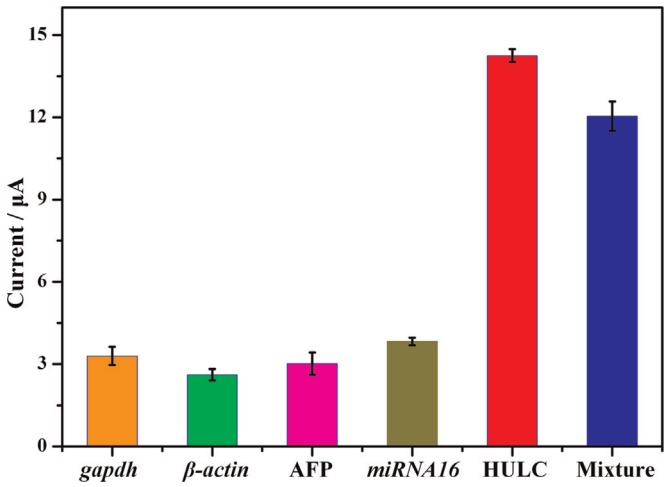

Fig. 5. Specificity of the proposed biosensor. *gapdh*: glyceraldehyde-3-phosphate dehydrogenase, AFP: alpha fetoprotein, HULC: highly up-regulated in liver cancer.

satisfactory detection limit and linear range.

3.7. Specificity, reproducibility, stability and reusability of the biosensor

To confirm whether the observed voltammetric response was generated from the capture-probe-HULC target-specific interaction or from a non-specific nucleotide interaction, we investigated the selectivity when the RNA biosensor was incubated with samples containing the following potential interfering substances: *gapdh*, *β-actin*, AFP, *miRNA16*, HULC and an HULC mixture. The presence of even 50-fold excess of the RNA (50 pM, *gapdh, β-actin, miRNA16*) and protein (1 nM AFP) causes minimal current responses, which are close to that of the blank test. However, the presence of the perfectly matched target lncRNA HULC and its mixture at an even lower concentration (50-fold, 1 pM) results in a significant increase in the current response (Fig. 5). This gap is statistically significant according to calculations performed using SPSS 19.0 ($P < 0.05$). The results reveal that the lncRNA biosensor exhibits ideal specificity.

The reproducibility of the proposed RNA biosensor was divided into intra-assay and inter-assay. The intra-assay was 4.27%, which was evaluated from the response of 1 pM/mL HULC at five different electrodes in the same batch. The inter-assay was investigated by analyzing a single HULC concentration (1 pM/mL) using five RNA biosensors made using the same electrode in batches. The relative standard deviation (R.S.D.) of the inter-assay was 2.91%. The results indicate that the developed RNA biosensor was excellent and could be used for lncRNA HULC analysis with acceptable reproducibility. Response time is the time required for reaching 95% of the equilibrium signal towards different catalytic material (Choi and Yiu, 2004; Gholivand and Khodadadian, 2014). The biosensor exhibited a rapid response to the changes in 0.8 mM H_2O_2 concentration in 2 s. But the stable DPV current can be obtained only after 15 s. And the response time of the biosensor was 15 s on going from 0.0 to 0.8 mM H_2O_2.

The stability of the RNA biosensor was evaluated for 28 days of storage at 4 °C and was measured every 3 days. The CV peak current of the RNA biosensor decreased gradually, and the final peak current retained 98.14% of the initial current after 21 days, demonstrating the acceptable stability of the RNA biosensor.

The reusability of the above HULC biosensor was analyzed via measuring binding with 1 pM HULC. After each measurement, the biosensor was regenerated upon de-hybridization in 94 °C hot water for most of nucleic acid duplexes can melt and the target and DP could drop off from biosensor in that temperature after washing three times (Stanley and Szewczuk, 2005; Wang et al., 2013). And the regenerated biosensor detected with CV method. After each cycle, current peak of the bare SWCNTs/Au/CP/HT/HULC electrode was found to decrease slightly (see Fig. S7 in the supplementary material). When current peak was calculated, the variation became even smaller. After 4 cycles of hybridization–dehybridization, the change is between 4.1% and 5.8% among the electrodes studied. Results indicate that the regeneration effect of the HULC biosensor is acceptable for HULC detection.

3.8. Detection of lncRNA HULC in clinical serum samples

The feasibility of the proposed RNA biosensor for clinical applications was investigated by standard addition methods in human serum. The samples were divided into 4 cases of HCC patients and 3 cases of healthy persons. We used *rt*-PCR to provide a quantitative comparison (Fig. S8). The results revealed satisfactory recoveries in the range of 0.89 pM/mL to 8.53 pM/mL. The results of the biosensor are very close to those detected by *rt*-PCR and could clearly distinguish groups between tumor and control. Results of the synthetic serum samples test obtained by the proposed biosensor are acceptable with recoveries between 97.1% and 101.7% (Table 1), which indicated that the proposed biosensor was feasible for the determination of lncRNA HULC and could satisfy the need for practical analyses.

4. Conclusions

We proposed a novel biosensor based on PtPd BND/BNF@GO and synchronous labeling of DP and thionine to detect lncRNA HULC. A PtPd BND/BNF@GO stereochemical structure was synthesized to regulate the surface structure of the catalysis material; the typical shape of the nanomaterial mainly consisted of a dendritic structure or mixed small part of a flower-like cluster. Because of the catalyst function of PtPd and the catalytic potentiation of the BND/BNF structure, PtPd BND/BNF@GO could enhance the catalytic efficiency and achieve triple-catalysis with HRP (Pt, Pd and HRP). The application of GO may prompt the loading amount of PtPd BND/BNF. Moreover, we adopted a strategy of

Table 1
Determination of lncRNA HULC in serum samples ($n=7$).

Serum sample	*rt*-PCR (relative expression)	Response (μA)	Observed concentration (pM/mL)	Expectation concentration in theory (pM/mL)	Relative standard deviation (%)	Recovery (%)
1	3.84	−19.15	3.49	3.43	3.2	101.7
2	4.31	−19.43	3.91	3.84	4.1	101.8
3	9.57	−20.65	8.53	8.56	5.9	99.6
4	1.45	−17.45	1.27	1.29	1.5	98.4
5	1.924	−17.99	1.75	1.72	2.0	101.7
6	3.43	−18.87	2.98	3.07	3.3	97.1
7	1.00	−16.84	0.89	0.95	2.7	93.7

synchronously and separately capping Au particles with thionine and detection probes, which clearly accelerated the modified time of the detection probe and decreased the electronic background. The experimental results confirmed that the proposed biosensor exhibited high sensitivity, good reproducibility, acceptable stability and ideal selectivity for the economical and fast quantitative detection of lncRNA HULC in the early diagnosis of HCC.

Acknowledgments

This work was supported by the National Natural Science Foundation of China (NSFC81401753, NSFC81472034, and NSFC81371898). We appreciate the valuable comments that we received from other members of our laboratory.

Appendix A. Supplementary material

Supplementary data associated with this article can be found in the online version at http://dx.doi.org/10.1016/j.bios.2015.06.021.

References

Bin, D., Ren, F.F., Wang, H.W., Zhang, K., Yang, B.B., Zhai, C.Y., Zhu, M.S., Yang, P., Du, Y.K., 2014. RSC Adv. 74, 39612–39618.
Centi, S., Laschi, S., Mascini, M., 2009. Bioanalysis 7, 1271–1291.
Choi, M.M.F., Yiu, T.P., 2004. Enzyme Microb. Technol. 1, 41–47.
Daniel, S., Rao, T.P., Rao, K.S., Rani, S.U., Naidu, G.R.K., Lee, H.Y., Kawai, T., 2007. Sens. Actuators B – Chem. 2, 672–682.
Doria, G., Conde, J., Veigas, B., Giestas, L., Almeida, C., Assuncao, M., Rosa, J., Baptista, P.V., 2012. Sensors (Basel) 2, 1657–1687.
Ferlay, J., Shin, H.R., Bray, F., Forman, D., Mathers, C., Parkin, D.M., 2010. Int. J. Cancer 12, 2893–2917.
Frens, G., 1973. Nat. Phys. Sci. 1, 20–22.
Gholivand, M.B., Khodadadian, M., 2014. Biosens. Bioelectron. 0, 472–478.
Gong, M.J., Han, T., Cai, C.X., Lu, T.H., Du, J.Y., 2008. J. Electroanal. Chem. 1, 8–14.
Guo, S.J., Dong, S.J., Wang, E.K., 2010. ACS Nano 1, 547–555.
He, P.A., Xu, Y., Fang, Y.Z., 2006. Microchim. Acta 3–4, 175–186.
Holford, T.R., Davis, F., Higson, S.P., 2012. Biosens. Bioelectron. 1, 12–24.
Jacobs, C.B., Peairs, M.J., Venton, B.J., 2010. Anal. Chim. Acta. 2, 105–127.
Lai, G.S., Yin, C.Y., Tan, X.G., Zhang, H.L., Yu, A.M., 2014. Anal. Methods (UK) 7, 2080–2085.
Li, Y., Deng, J., Fang, L.C., Yu, K.K., Huang, H., Jiang, L.L., Liang, W.B., Zheng, J.S., 2015. Biosens. Bioelectron. 63, 1–6.
Liang, H.P., Zhang, H.M., Hu, J.S., Guo, Y.G., Wan, L.J., Bai, C.L., 2004. Angew. Chem. Int. Ed. 12, 1540–1543.
Lim, B., Jiang, M.J., Camargo, P.H.C., Cho, E.C., Tao, J., Lu, X.M., Zhu, Y.M., Xia, Y.N., 2009. Science 5932, 1302–1305.
Liu, S.N., Wu, P., Li, W., Zhang, H., Cai, C.X., 2011. Anal. Chem. 12, 4752–4758.
Liu, W.Y., Yang, H.M., Ge, S.G., Shen, L., Yu, J.H., Yan, M., Huang, J.D., 2015. Sens. Actuators B – Chem. 209, 32–39.
Liu, X.H., Zhang, R., Yuan, X.Q., Liu, L., Zhou, Y.Y., Gao, Q., 2014. Gold Bull. 1–2, 119–125.
Lv, J.-J., Zheng, J.-N., Zhang, H.-B., Lin, M., Wang, A.-J., Chen, J.-R., Feng, J.-J., 2014. J. Power Sour. 0, 136–143.
Panzitt, K., Tschernatsch, M.M., Guelly, C., Moustafa, T., Stradner, M., Strohmaier, H. M., Buck, C.R., Denk, H., Schroeder, R., Trauner, M., Zatloukal, K., 2007. Gastroenterology 1, 330–342.
Shao, Y.Y., Wang, J., Wu, H., Liu, J., Aksay, I.A., Lin, Y.H., 2010. Electroanal 10, 1027–1036.
Shin, H.S., Yang, H.J., Kim, S.B., Lee, M.S., 2004. J. Colloid Interface Sci. 1, 89–94.
Siegel, R., Ma, J., Zou, Z., Jemal, A., 2014. CA: Cancer J. Clin. 1, 9–29.
Stanley, K.K., Szewczuk, E., 2005. Nucleic Acids Res. 20, e180.
Tang, D.P., Yuan, R., Chal, Y.Q., 2008. Anal. Chem. 5, 1582–1588.
Vasquez, Y., Sra, A.K., Schaak, R.E., 2005. J. Am. Chem. Soc. 36, 12504–12505.
Wang, J., 2012. Microchim. Acta 3–4, 245–270.
Wang, L., Nemoto, Y., Yamauchi, Y., 2011. J. Am. Chem. Soc. 25, 9674–9677.
Wang, S., Li, L., Jin, H.L., Yang, T., Bao, W.W., Huang, S.M., Wang, J.C., 2013. Biosens. Bioelectron. 41, 205–210.
Wu, X., Chai, Y., Yuan, R., Su, H., Han, J., 2013. Analyst 4, 1060–1066.
Xie, H., Ma, H., Zhou, D., 2013. Biomed. Res. Int. 2013, 136106.
Yang, C.Y., Wang, Q., Xiang, Y., Yuan, R., Chai, Y.Q., 2014. Sens. Actuators B – Chem. 197, 149–154.
Yuan, S.X., Yang, F., Yang, Y., Tao, Q.F., Zhang, J., Huang, G., Wang, R.Y., Yang, S., Huo, X.S., Zhang, L., Wang, F., Sun, S.H., Zhou, W.P., 2012. Hepatology 6, 2231–2241.
Yuan, Y.L., Yuan, R., Chai, Y.Q., Zhuo, Y., Liu, Z.Y., Mao, L., Guan, S., Qian, X.Q., 2010. Anal. Chim. Acta 2, 171–176.
Zhang, L., Zhang, J.W., Kuang, Q., Xie, S.F., Jiang, Z.Y., Xie, Z.X., Zheng, L.S., 2011. J. Am. Chem. Soc. 43, 17114–17117.
Zhou, K.B., Li, Y.D., 2012. Angew. Chem. Int. Ed. 3, 602–613.
Zhu, L., Luo, L., Wang, Z., 2012. Biosens. Bioelectron. 1, 507–511.
Zhu, X., Niu, X., Zhao, H., Tang, J., Lan, M., 2015. Biosens. Bioelectron. 67, 79–85.